Journal of Constructional Steel Research 151 (2018) 12–24

Contents lists available at ScienceDirect

Journal of Constructional Steel Research

Flexural strength evaluation of concrete-filled steel tube (CFST) composite girder

Junghyun Cho [a], Jiho Moon [b,*], Hee-Jung Ko [c], Hak-Eun Lee [a]

[a] School of Civil, Environmental & Architectural Engineering, Korea University, Seoul 02841, Republic of Korea
[b] Dept. of Civil Engineering, Kangwon National University, Chuncheon-si, Gangwon-do 24341, Republic of Korea
[c] MIDAS IT, Seongnam-si, Gyeonggi-do 13487, Republic of Korea

ARTICLE INFO

Article history:
Received 30 March 2018
Received in revised form 30 June 2018
Accepted 31 August 2018
Available online xxxx

Keywords:
Concrete-filled steel tube (CFST)
Composite girder
Flexural strength
Steel-concrete composite structure

ABSTRACT

The flexural strength of the concrete-filled steel tube (CFST) composite girder was investigated in this study. Firstly, simple equations to evaluate the flexural strength of the CFST composite girder under both positive and negative bending moment were derived based on the plastic stress distribution method (PSDM). A series of tests was then conducted to verify the accuracy of the proposed equation, and to investigate the effect of internal shear connectors between the steel tube and concrete infill. Further, non-linear finite element analysis for each test specimen was performed to demonstrate the failure mechanism, and to set up the verified finite element analysis model. From the results, it was found that the proposed equations provided a reasonably conservative prediction of the flexural strength of the CFST composite girder under both positive and negative bending moment, and the effect of internal shear connectors between the steel tube and concrete infill on the flexural strength was negligible. A series of parametric studies was performed to investigate the effect of the D/t ratio, compressive strength of the concrete infill, and local buckling of the steel tube on the flexural strength of the CFST composite girder. Finally, some design considerations are noted based on the results of the parametric study.

1. Introduction

The concrete-filled steel tube (CFST) is a composite member that consists of steel tube and concrete infill. The major benefit of the CFST is that the concrete infill is confined by the tube resulting in a tri-axial state of compression that increases the strength and strain capacity of the concrete [1,2]. In particular, when subjected to cyclic axial or flexural loading conditions, the crushed concrete remains confined within the steel tube, providing high ductility and energy dissipation with delayed degradation of resistance [3,4]. Furthermore, the concrete infill restrains buckling deformation of the tube, and leads to an increase in buckling strength [5]. To take these benefits, CFSTs have been widely used as building columns and bridge piers, where the major loading is axial compression. Recently, the applications of the CFST have been extended to the superstructure of bridges.

Chen and Wang [6] reported that CFST arch bridges have been built more than 200 since 1990 in China, and the CFST bridges become a good alternative to reinforced concrete bridges or steel bridges due to the structural advantages and artistic appearance of the CFST. Recently, CFSTs have also been used as parts of a girder to adopt the ability to provide strength, ductility, constructability and aesthetic [7–11], and the CFST composite girder system was first proposed by Nakamura et al. [7].

Fig. 1 shows a typical CFST composite girder. The CFST composite girder consists of CFST and concrete slabs, and these are connected with mechanical shear connectors. By replacing the conventional I-girder with a CFST, the noise and vibration induced by cars or trains, which are the major disadvantages of a conventional steel I-girder bridge, can be reduced [9]. And it can also be expected that the local and global instability resistance of the bridge increases by using CFSTs. In the construction of the CFST composite bridge, steel tubes are produced at steel mill, thus little fabrication is required to make them bridge girders, and the steel tube serves as a formwork so that the labor associated with formwork can be reduced [6,9–11]. Therefore, the CFST composite girder could be economical compared with conventional welded plate girders.

Despite these benefits, the use of CFSTs in girder bridge systems has been limited since design methods for CFST composite girders are not yet well established. Design provisions for CFST components are available in some design codes such as AISC [12]. Further, many studies [5,13–18] have been conducted to investigate the flexural behavior of CFST components. However, there are clear differences between a CFST component and a CFST composite girder. For example, a concrete

* Corresponding author.
E-mail address: jmoon1979@kangwon.ac.kr (J. Moon).

https://doi.org/10.1016/j.jcsr.2018.08.038
0143-974X/

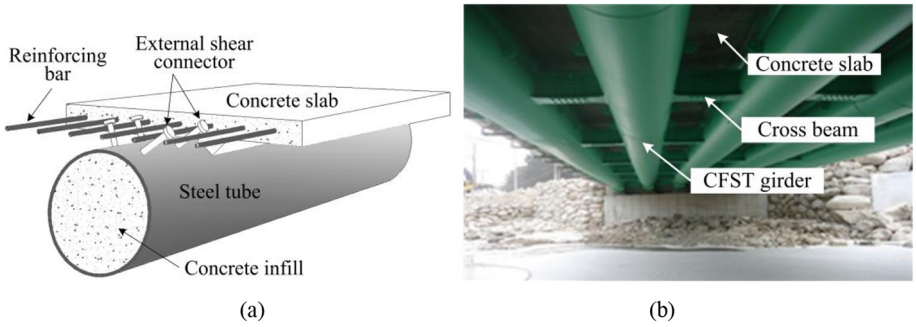

Fig. 1. Typical CFST composite girder: (a) Schematic view of CFST composite girder, and (b) Construction example.

slab is connected to a CFST with mechanical shear connectors, and it should be considered to evaluate the flexural strength of such a girder. The major loading of a CFST composite girder is bending moment, and the D/t ratio is an important parameter that affects the flexural behavior of the CFST composite girder, where D is the outer diameter of the steel tube, and t is the thickness of the steel tube. A low D/t ratio may result in brittle failure in the concrete slab of a CFST composite girder, since the reinforcement ratio of a CFST composite girder increases with decreasing D/t ratio. Thus, it is important to thoroughly understand the flexural behavior of the CFST composite girder considering these key parameters.

In this study, the flexural strength of the CFST composite girder was investigated. Simple equations to evaluate the flexural strength of the CFST composite girder were proposed for both positive and negative bending. The experimental study was then performed to examine the validation of the proposed equations. Also, the effect of internal shear connectors between the steel tube and concrete infill on the flexural strength of such girder was investigated through a series of tests. Finite element analysis was conducted for each test specimen to demonstrate the strain distribution of test specimens in depth, and to develop the verified finite element analysis model for parametric study. A series of parametric studies was conducted to investigate the effects of the D/t ratio, compressive strength of the concrete infill, and local buckling of the steel tube on the flexural strength of the CFST composite girder. Finally, some design considerations are discussed based on the results of this parametric study.

2. Simplified equation to predict the flexural strength of a CFST composite girder

The AISC design code [12] provides two different methods to evaluate the strength of a composite section: (1) the plastic stress distribution method (PSDM), and (2) the strain compatibility method (SCM). The PSDM assumes that the steel part reaches full yield stress, f_y, in either tension or compression at the ultimate state, while the concrete part in compression achieves a stress of 0.95 f_c' for a circular CFST, where f_c' is the compressive strength of concrete, and the contribution of the concrete in the tension part is neglected. In the case of the SCM, a linear distribution of strains across the section is assumed for the ultimate state with the maximum concrete compressive strain of 0.003. Although a computational procedure of the ultimate strength by the SCM is generally more complicated than the PSDM, it was reported that the PSDM provides a reliable and simple method to estimate the flexural strength of the CFST [13]. Thus, the PSDM was used to derive the equations to predict the flexural strength of the CFST composite girder in this study.

Fig. 2 shows the plastic stress distribution of a CFST composite girder under positive bending moment for various locations of the plastic neutral axis (PNA). The PNA is located in concrete slab, steel tube, and concrete infill for case 1, 2, and 3, respectively. It should be noted that the reduction factor for the compressive strength of concrete is adopted as 0.95 and 0.85 for the concrete infill and concrete slab, respectively, according to AISC [12]. In Fig. 2, b_e is the effective width of the slab, d is the depth of the reinforcing bar, a is the depth of the compressive concrete stress block, t_c is the thickness of the slab, h_r is the gap between the slab and CFST, r_i is the inner radius of the tube, r_m is the mean radius of the tube, R is the outer radius of the tube, t is the thickness of the tube, y_2 is the distance from the top of CFST to the compressive force of the slab, G_d is the distance from the center of the CFST to the reinforcing bar, $\overline{y}$ is the distance from the top of the CFST to the PNA, G_s is the distance from the center of the CFST to the centroid of the compression zone of the tube, G_i is the distance from the center of the CFST to the centroid of the compression zone of the concrete infill, f_{cc}' is the compressive strength of the concrete slab, f_{ci}' is the compressive strength of the concrete infill, f_y is the yield stress of the steel tube, C_c is the compressive force of the slab, C_s is the compressive force of the tube, C_i is the compressive force of the concrete infill, F_r is the compressive force in the reinforcing bar, T is the tensile force of the tube, and P_y is the yield force of the whole section of the tube.

By assuming the plastic stress distribution shown in Fig. 2, the flexural strength of the CFST composite girder, M_u, under positive bending moment can be simply obtained as follows:

$$\begin{aligned} &Case1: M_u = C_c(R + y_c - 0.5a) \quad \text{(a)} \\ &Case2: M_u = C_c(y_2 + R - G_s) + P_y G_s + F_r(G_d - G_s) \quad \text{(b)} \\ &Case3: M_u = C_c(y_2 + R) + 2C_s G_s + C_i G_i + F_r G_d \quad \text{(c)} \end{aligned} \tag{1}$$

The complete form of the proposed Eq. (1) is shown in appendix I. It should be noted that the contribution of the reinforcing bar on the flexural strength was neglected for case 1, since the distance between the reinforcing bar and the PNA is negligibly small compared with the other dimensions. It is also noted that the location of the PNA should be evaluated first to apply Eq. (1). The location of the PNA can be calculated from the force equilibrium of the section (i.e. the axial force acting on the section is equal to zero).

In the case of the CFST composite girder under negative bending moment, the whole section of the slab is subjected to tension, and it is neglected. Further, it is assumed that the PNA locates in the concrete infill. Thus, M_u can be obtained by modifying Eq. (1-c), where C_c in Eq. (1-c) is equal to zero. As a result, M_u in the negative moment region is given by.

$$M_u = 2C_s G_s + C_i G_i + F_r G_d. \tag{2}$$

The complete form of the proposed Eq. (2) is also shown in appendix I.

3. Experimental study

3.1. Objectives of the experimental study

A series of experimental studies was conducted for two different objectives. The first one was to examine the validation of the proposed

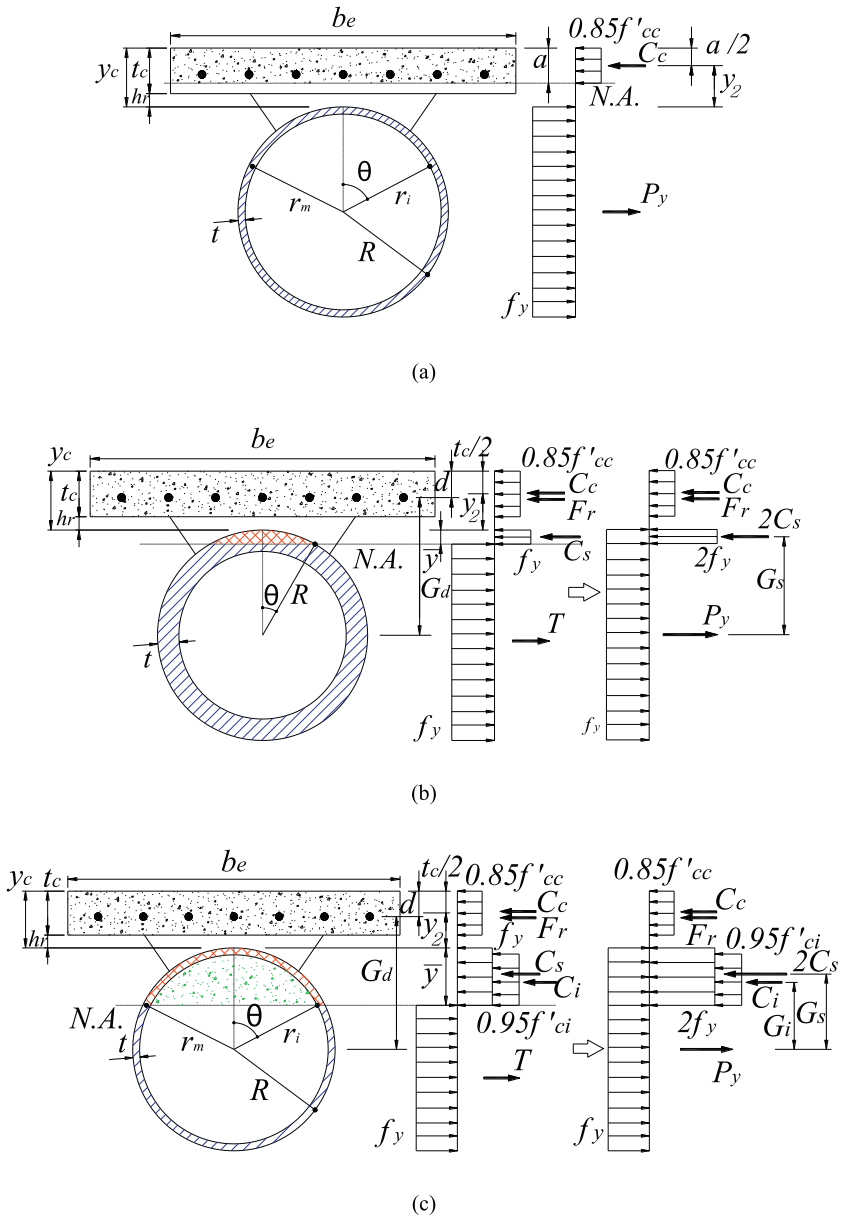

Fig. 2. Plastic stress distribution for various locations of PNA: (a) case 1 (PNA in the slab), (b) case 2 (PNA in the steel tube), and (c) case 3 (PNA in the concrete infill).

equations. The second objective was to investigate the effect of internal shear connectors on the flexural strength of the CFST composite girder. Internal shear connectors between the steel tube and concrete infill are often used to enhance the composite action between the steel tube and concrete infill. However, the concrete infill of the CFST composite girder mostly undergoes tension, and it is expected that the concrete infill may not affect the flexural strength of the CFST composite girder significantly, even though it is helpful to retain the original cross section shape under lateral loading. For these objectives, three large-scale CFST composite girder specimens were constructed and tested.

3.2. Description of specimens and test setup

Fig. 3 shows the dimensions of the three test specimens (SC-P, FC-P, and FC-N). All test specimens had the same profiles of CFST and concrete slab. The dimensions were determined based on the profiles of existing bridges with CFST composite girder constructed in Japan & South Korea and the specimens tested by previous researcher [11], as shown in Table 1. In Table1, b_e represents the effective width of the slab. The outer diameter of the CFST was 355.6 mm, which is the same with the test specimen of Yoshida et al. [11], and the thickness of the tube was 4.5 mm. This results in a D/t ratio of 79, which is equivalent to a reinforcement ratio ρ of 5%. From Table 1, it can be seen that the ratio between the width of the slab and the diameter of the steel tube varies from 1.7 to 1.9. For thickness of the slab / diameter of the steel tube ratio, it ranges from 0.19 to 0.28. Based on these values, width of the slab / diameter of the steel tube ratio and thickness of the slab / diameter of the steel tube ratio were determined as 2 and 0.25 for the test specimens, respectively. Therefore the width and thickness of the concrete slab were 700 mm and 90 mm, respectively.

Positive bending moment was applied to SC-P and FC-P specimens, while FC-N was subjected to negative bending moment. Internal shear connectors were installed between the steel tube and concrete infill for the SC-P specimen, while they were not for the other specimens (FC-P & FC-N). Generally, the condition of full shear connection for the composite girder can be satisfied if the nominal shear strength of shear connectors, $\sum Q_n$, is larger than the minimum of P_c ($= 0.85 f_{cc}' A_c$) and P_t ($= A_s f_y$), where P_c is the axial strength of the

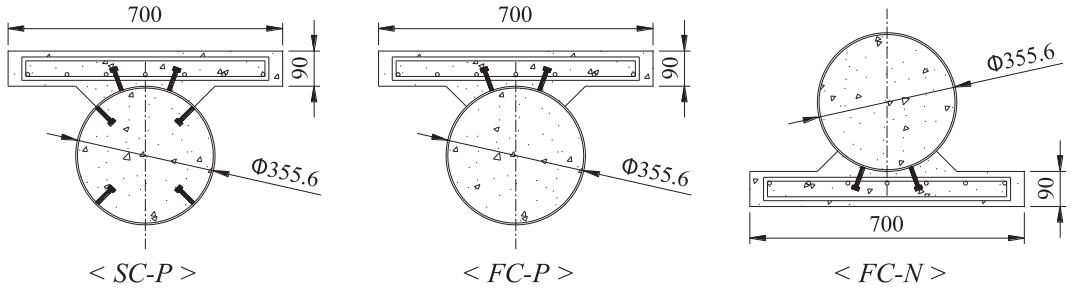

Fig. 3. Profiles of test specimens (unit: mm).

Table 1
Profiles of existing bridges with CFST composite girder and specimens tested by previous researchers.

Name of bridge or researchers	Slab (mm)		Steel tube (mm)		D/t	f_c' (MPa)		f_y (MPa)
	b_e	thick.	dia.	thick.		slab	infill	
Samil 1 bridge (S. Korea)	1900	240	1000	16–28	56.7–60.6	27	27	460
Hokurikudo over bridge (Japan)	2500	250	1320	22	60	35	5–27	500
Yoshida et al. (2001) [11]	600	100	355.6	6.4	56	40	40	345

concrete slab and P_t is that of the steel element. It should be noted that sufficient shear connectors between the concrete slab and CFST were installed to ensure full composite action according to AASHTO [19] for all specimens. The diameter and length of the shear connecter were 13 mm and 52 mm, respectively. The ultimate tensile strength of the shear connector was 420 MPa. The measured yield stress of the steel tube was 244.1 MPa, and the measured compressive strength of the concrete infill and slab were 40.9 and 24.4 MPa, respectively.

The test setup used in this study is shown in Fig. 4. A concentrated load was applied at the mid-span of the test specimens, where the girder was simply supported with a span of 3850 mm. A linear variable displacement transducer (LVDT) was placed at mid-span to measure vertical deflection, and strain gages were attached on the surface of the steel tube and reinforcing bars to measure strain data, as shown in Fig. 5.

3.3. Test results (SC-P & FC-P specimens)

The relationships between the normalized moment and deflection for the SC-P and FC-P specimens are shown in Fig. 6. In Fig. 6, normalized deflection, defined as the mid-span deflection divided by half span of the girder is plotted on the x axis while the y axis is plotted, the applied moment normalized by the flexural strength from the PSDM, $M_{u,PSDM}$, obtained from Eq. (1). M_{yb}, M_{ym}, and M_{yt} in Fig. 6 are moments corresponding to yielding of the bottom, mid-height and top of the steel tube, respectively.

From the results, it was seen that the stiffness was considerably reduced when the bottom of the steel tube yielded (M_{yb}), and the flexural strength $M_{u,test}$ was very close to M_{yt}, for both SC-P and FC-P specimens. In addition, the relationships between the normalized moment and deflection for the SC-P and FC-P specimens are almost identical, and the effect of internal shear connectors between the steel tube and concrete infill on the flexural strength was insignificant for the CFST composite girder under positive bending moment. From the test results, flexural strength obtained from the test, $M_{u,test}$, was observed at around 2.5% normalized deflection for both specimens. $M_{u,test}$ were 372.772 kN·m and 376.222 kN·m for the SC-P and FC-P specimens, respectively. The theoretical strength of the test specimens is 277.386 kN·m for both the SC-P and FC-P specimens, since the effect of the internal shear stud is not considered in the proposed equations. The proposed equations underestimated the flexural strength of SC-P and FC-P by approximately 25.6% and 26.3%, respectively. It should be noted that the theoretical strength of the CFST alone without the concrete slab is calculated as 174.689 kN·m for the test CFST section. Thus, there are 58.79% flexural strength increase comparing to the theoretical strength of the CFST composite girder, and the contribution of the concrete slab to the flexural strength is significant.

Figs. 7 and 8 show the strain and stress distributions at 2.5% normalized deflection for the SC-P and FC-P specimens, respectively. From these strain distributions obtained from the test (Figs. 7 (a) and 8 (a)), it can be seen that the strain at the bottom and the top of the steel tube exceeded the yield strain, ε_y ($\varepsilon_y = 0.001357$). On the other hand,

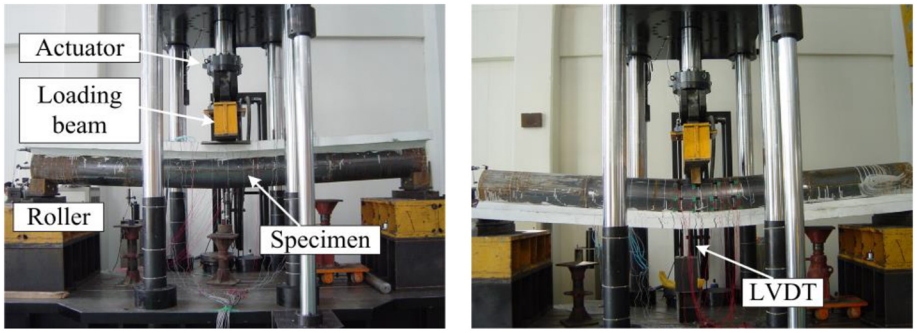

Fig. 4. Test setup: (a) for the SC-P and FC-P specimens, and (b) for the FC-N specimen.

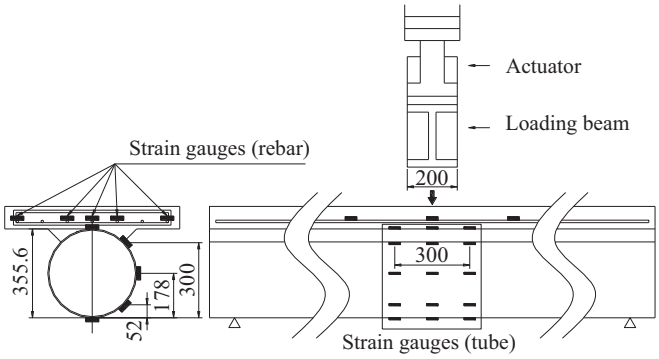

Fig. 5. Arrangement of the strain gauges.

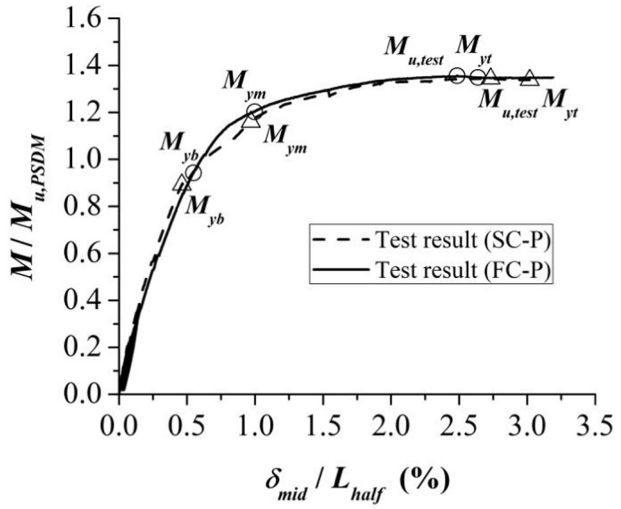

Fig. 6. Normalized moment-deflection relationship for the SC-P and FC-P specimens.

the strains of the reinforcing bar and concrete surface were smaller than those of the steel tube. Further, a discontinuity in strain distribution was observed at the interface between the steel tube and concrete slab. This is attributed to the slip at the interface, and it implies that the test specimens (SC-P & FC-P) showed partial interaction behaviors. During the test, there is no shear stud failure. However, the cracks and slip between the CFST tube and concrete slab was observed. Fig. 9 shows the slip and cracks at the end of the specimen after test.

Even though the discontinuity in strain distribution was observed, the PSDM is still available, since the whole concrete slab undergoes compression, and there is only one neutral axis in the composite section. Generally, full shear connection can be ensured regardless of the degree of interaction, when there is one neutral axis on the composite section according to Oehlers & Bradford [20]. Clearly, the SCM may not be appropriate to evaluate the flexural strength of the composite girder with a partial interaction system due to the discontinuous strain distribution. The effect of the degree of interaction on the flexural strength for the test specimen will be discussed in Section 4.

Based on the strain distributions shown in Figs. 7 (a) and 8 (a), the stress distributions were obtained, as shown in Figs. 7 (b) and 8 (b), for the SC-P and FC-P specimens. The dashed lines in Figs. 7 (b) and 8 (b) represents the idealized plastic stress distributions from the PSDM. It is noted that the uniaxial stress-strain relationship obtained from the material test was used to convert the strain distribution to stress distribution for simplicity. The stress near the neutral axis (NA) didn't reach f_y, while the stress of the steel tube in tension region was larger than f_y due to strain hardening, as shown in Figs. 7 (b) and 8 (b). However, the overall stress distribution obtained from the test was similar to that from the PSDM. In addition, the effect of internal shear connectors between the steel tube and concrete slab on the strain and stress distribution was negligible. The flexural strengths were calculated, based on the stress distributions obtained from the tests shown in Figs. 7 (b) and 8 (b). The calculated flexural strengths were 309.33 kN·m and 296.06 kN·m for SC-P and FC-P specimens, respectively. These values are approximately 10% higher than that from the PSDM. This resulted from the strain hardening and increased moment arm. However, these predicted values are still 20% smaller than the flexural strengths obtained from the moment- deflection relationship (M_u from the tests were 372.772 kN·m and 376.222 kN·m for SC-P and FC-P specimens, respectively). This discrepancy may be caused by the multi-axial effects on the stress and the confinement effects near the loading point were neglected when the strain distribution was converted into stress distribution.

The crack patterns of concrete infill for the SC-P and FC-P specimens were documented after testing by removing the steel tube, as shown in Fig. 10. The whole section of concrete infill was cracked for both test specimens. This means that most of the concrete infill undergoes tension, and it has insignificant effects on the flexural behavior. In the case of the SC-P specimen, major cracks were developed at the point of the internal shear connectors, while uniformly distributed light hairline cracks were observed in the FC-P specimen. Taken as a whole, it can be found that the internal shear connectors between the concrete slab and concrete infill have insignificant effect on the flexural strength, strain and stress distribution, while they affect the cracking pattern of the concrete infill when most concrete infill experiences tension.

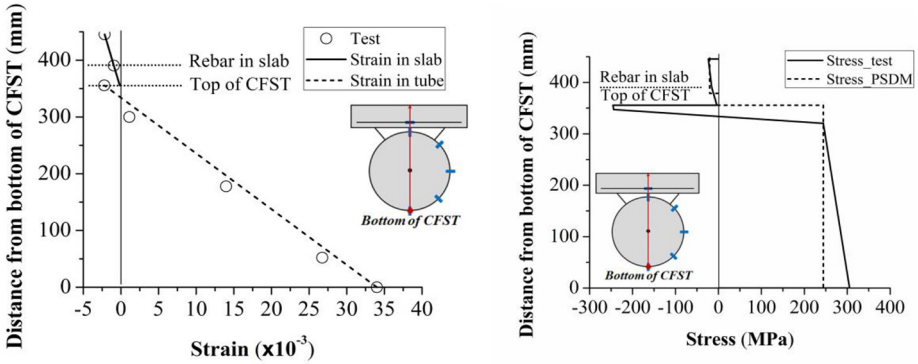

(a) (b)

Fig. 7. Strain & Stress distribution of the SC-P specimen at 2.5% normalized deflection: (a) strain distribution, and (b) stress distribution.

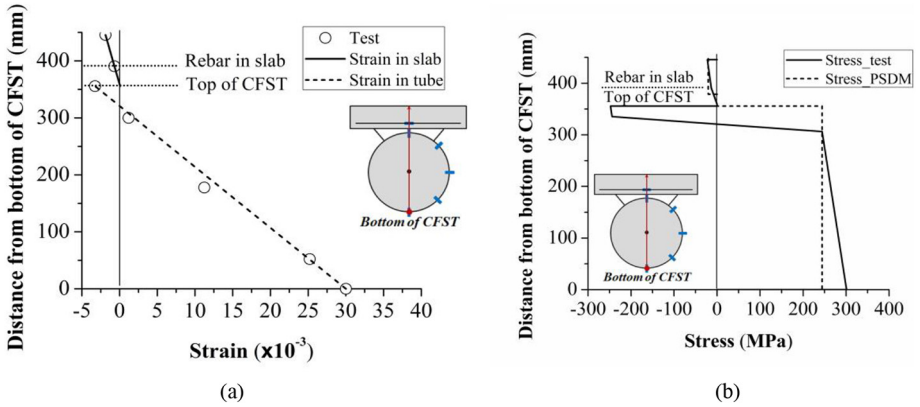

Fig. 8. Strain & Stress distribution of the FC-P specimen at 2.5% normalized deflection: (a) strain distribution, and (b) stress distribution.

3.4. Test results (FC-N specimen)

Fig. 11 shows the relationship between the normalized moment and deflection of the FC-N specimen. In Fig. 11, M_{yr} is the moment corresponding to yielding of the rebar, and M_{lb} represents the moment when local buckling occurs. The $M_{u,test}$ observed around at 6% normalized deflection, and the $M_{u,test}$ was 328.01 kN·m. The theoretical strength from the proposed equation was 251.12 kN·m, and the proposed equation underestimated the test results by approximately 23.4%. As mentioned before, the theoretical strength of the CFST alone is 174.689 kN·m for the test CFST section. Thus, for the negative bending, the contribution of the concrete slab to the theoretical flexural strength is approximately 43.75% for the tested composite section. It is smaller than the positive bending case, but still the effect of the concrete slab on the flexural strength is significant.

Local buckling was observed near the loading region at around 3% normalized deflection, as shown in Fig. 12. At 3% normalized deflection, the whole section of steel tube yielded, as shown in Fig. 11. Thus, this local buckling was caused by the yielding of the top surface of the steel tube. Even though local bucking was observed at 3% normalized deflection, the moment resistance was continuously increased up to 6% normalized deflection, and the specimen shows ductile behavior, as show in Fig. 11.

Fig. 13 (a) shows the strain distributions at 0.8% and 6% normalized deflection of the FC-N specimen. The strain distributions were almost linear without any discontinuity at both 0.8% and 6% normalized deflections. Fig. 13 (b) represents the stress distribution of the FC-N specimen at 6% normalized deflection, which was converted from the strain distribution shown in Fig. 13 (a) by using the uniaxial stress-strain relationship obtained from the material tests. The stress distribution obtained from the test was very close to that from the PSDM except for the strain hardening effect. This is because the strain distribution was almost linear without any discontinuity. Further, there is slip between the CFST tube and the concrete slab and cracks were not observed at the end of the test specimen during the test, as shown in Fig. 14. The moment resistance calculated from the stress distribution was 275.72 kN·m, and it was 9.8% more conservative than that from the PSDM.

Similarly to the positive bending test specimens, crack patterns were observed for the FC-N specimen, as shown in Fig. 15. Flexural cracks were observed up to the neutral axis, and the concrete parts at the local buckling region were crushed, since the confinement effect cannot be expected in a buckled region.

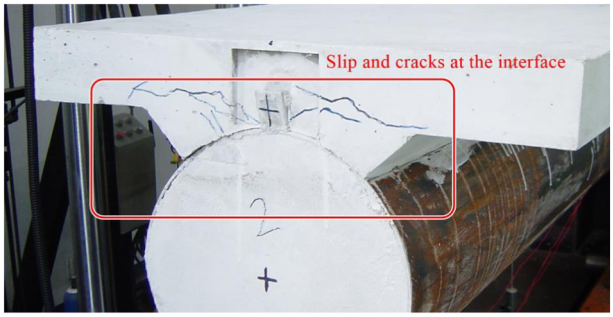

Fig. 9. Slip and cracks at the end of the test specimen (FC-P, After test).

4. Finite element analysis of the CFT composite girder for test specimens

4.1. Description of the finite element model

Finite element analyses were conducted for each test specimen to investigate the strain distribution in depth, and to set up the verified finite element model for parametric study. Several researchers have conducted finite element analysis to investigate the behavior of the CFST component, and most of them use the empirically established confined constitutive law for the concrete infill [1,2,21]. In this study, the confinement effect was directly modeled by using the stress-strain relationship of un-confined concrete, and the GAP element provided by ABAQUS [22]. This approach was previously used by Moon et al. [5], and the model was verified under various loading conditions. The GAP element in ABAUQS [22] has no tensile resistance so that separation of two nodes can be modeled, while it prevents penetration of the node into the adjacent one. Thus, the compression developed in the GAP element provides the confinement stress to the concrete infill. Also, a friction coefficient can be assigned to the GAP element, and it provides the shear stress that is needed to develop the composite action between the steel tube and concrete infill.

Fig. 16 shows the typical finite element analysis model for the CFST composite girder used in this study. A quarter model was used to save computing time. An 8-node continuum element with reduced integration was used to model the concrete infill and slab. A 2-node truss and 4-node shell element were adopted for the reinforcing bar and steel tube, respectively. To simulate the internal and external shear connectors, 3-dimensional non-linear spring elements were used. Also, a GAP element was used to simulate the interface between the steel tube and concrete infill, as mentioned before. Baltay & Gjelsvik [23] reported that the friction coefficient between the steel and concrete varies from 0.3 to 0.6. A series of parametric studies was performed to determine the proper friction coefficient. Friction coefficients of 0.47 and 0.6 gave a best match with the positive and negative bending moment test results, respectively, and these values were used in this study.

Fig. 10. Crack pattern of the concrete infill: (a) SC-P specimen; and (b) FC-P specimen.

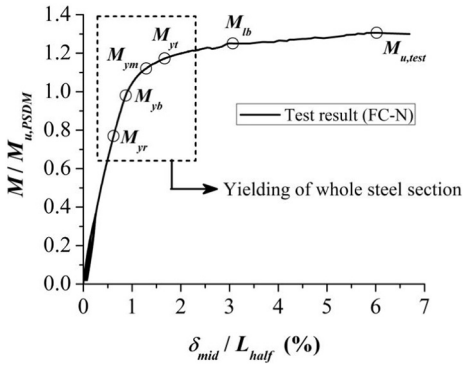

Fig. 11. Normalized moment-deflection relationship for the FC-N specimen.

The un-confined uniaxial compressive stress-strain curve was assumed to follow a parabolic curve, and it is given by.

$$f_c = f_c' \left\{ 2\frac{\varepsilon_c}{\varepsilon_c'} - \left(\frac{\varepsilon_c}{\varepsilon_c'}\right)^2 \right\}. \quad (3)$$

where, f_c' is the compressive strength of concrete, and ε_c' is the strain corresponding to f_c'. ε_c' was taken as 0.003 in this study. For the tensile behavior of the concrete, the tension softening model proposed by Hsu & Mo [24] was adopted, and the model is given by.

$$\begin{aligned} f_c &= E_c\varepsilon_c \quad \text{(a)} \\ f_c &= f_{cr}(\varepsilon_{cr}/\varepsilon_c)^{0.4} \quad \text{(b)} \end{aligned} \quad (4)$$

where, E_c is the young's modulus of the concrete, f_{cr} is the cracking stress of the concrete, and ε_{cr} is the cracking strain of the concrete. To simulate the inelastic behavior of the concrete, a damaged concrete plasticity model [22] was used. For this model, the dilation angle is an important parameter that governs the inelastic behavior of the concrete. 20 and 31 degree of dilation angles were used for the concrete infill and concrete slab, respectively, based on the results of a previous researcher [5]. In the case of steel tube, the measured stress-strain curve was used for the analysis.

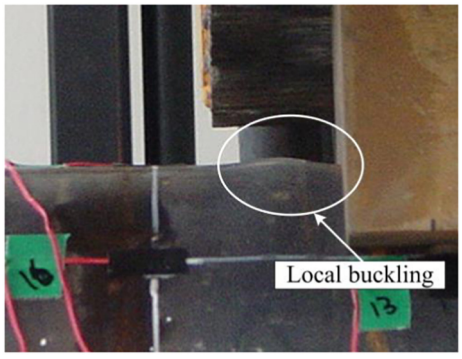

Fig. 12. Local buckling of the steel tube.

The behavior of embedded rebar is quite different from that of bare rebar. The major difference is the lowering of yield stress due to stress concentration in the rebar around the crack. To simulate this behavior, the average stress-strain relationship of embedded rebar proposed by Hsu & Mo [24] was used. The mathematical expression of this relationship is as follows:

$$\begin{aligned} f_s &= E_s\varepsilon_s \text{ when } \varepsilon_s \le \varepsilon_y' \quad \text{(a)} \\ f_s &= (0.91-2B)f_y + (0.2+0.25B)E_s\varepsilon_s \text{ when } \varepsilon_s > \varepsilon_y' \quad \text{(b)} \end{aligned} \quad (5)$$

in which,

$$\begin{aligned} &\varepsilon_y' = f_y'/E_s, \; f_y' = (0.93-2B)f_y \quad \text{(a)} \\ &B = 1/\rho\left(f_{cr}/f_y\right)^{1.5} \text{ when } \rho \ge 0.15\% \quad \text{(b)} \end{aligned} \quad (6)$$

The stiffness and strength of the shear connector is one of the important parameters that affect the behavior of composite structure. In this study, a parametric study was conducted to determine the proper model of the load-slip relationship for the CFST composite girder. The load-slip relationship of the shear connector proposed by Oehler & Coughlan [25] and Shima & Watanabe [26], shown in Fig. 17, were examined. A series of the finite element analyses was conducted for the test specimens with these two models. From the analysis results, the finite element analysis model with the load-slip curve of Shima & Watanabe [26] shows the better correlation with the test results, and it was adopted in this study. The load-slip relationship model proposed by Shima & Watanabe [26] is given by.

$$P_s = P_u\left(1-e^{-\alpha\delta/d_s}\right)^{2.5}, \; \alpha = 11.5\left\{1.1(\gamma-1)^2+1\right\}f_c'/30 \quad (7)$$

where P_s is the shear force acting on the connector, P_u is the shear strength of one shear connector, δ is the slip, d_s is the diameter of the shear connector, f_c' is the compressive strength of concrete (MPa), and γ is obtained from.

$$\gamma = \frac{A_{ss}f_{su}}{31A_{ss}\sqrt{f_c'h_s/d_s}+10000} \quad (8)$$

In Eq. (8), A_{ss} is the cross-sectional area of a shear connector (mm^2), f_{su} is the tensile strength of the shear connector (MPa), and h_s is the height of the shear connector.

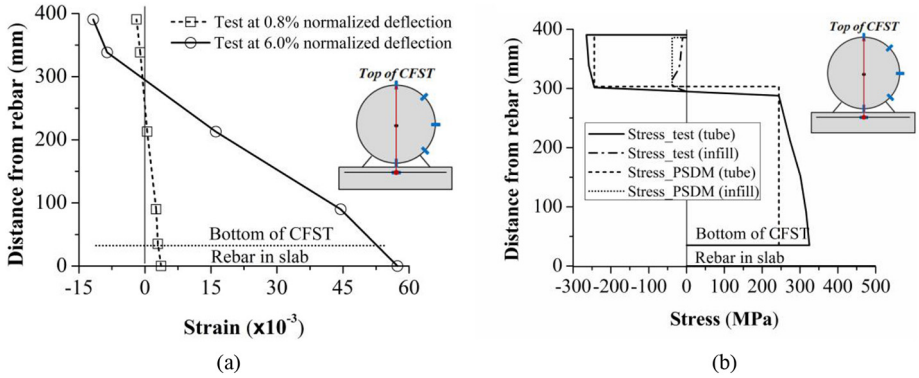

Fig. 13. Strain & Stress distribution of the FC-N specimen: (a) strain distribution at 0.8% and 6% normalized deflection, and (b) stress distribution at 6% normalized deflection.

Fig. 14. Slip and cracks at the end of the test specimen (FC-N, Final stage).

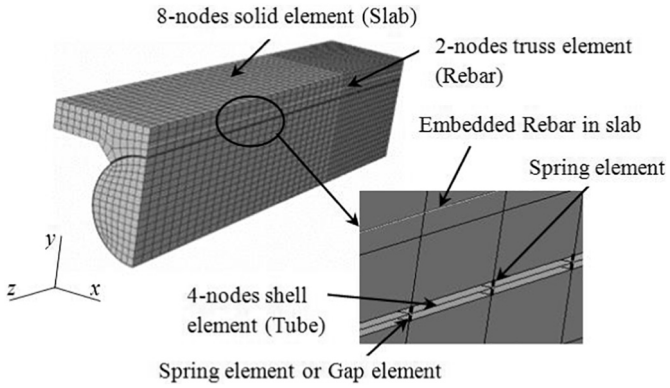

Fig. 16. FE model for the CFST composite girder.

The load and boundary conditions are shown in Fig. 18. The *x*-*y* plane at the mid-span of the model was restrained in the *z* direction, and the *y*-*z* plane at the center of the model was constrained in the *x* direction considering symmetry. Displacement loads were applied at the mid-span, where the load was applied at the top of the concrete slab and bottom of the steel tube for the positive and negative bending test model, respectively. The ends of the analysis models were constrained in the *y* direction, as shown in Fig. 18, where the bottom of the steel tube and the top of the concrete slab were constrained for the positive and negative bending test models, respectively.

4.2. Verification of the FE model, and discussion of the analysis results

Fig. 19 provides a comparison of the analysis results with the test. The *x* and *y* axes in Figs. 19 (a)–(c) represent the normalized deflection and normalized moment, respectively. The analysis results agree well with the test for all specimens. From the analysis results, the finite element models underestimated the flexural strength of the SC-P, FC-P, and FC-N specimen by 7%, 8%, and 10%, respectively. It is noted that the applied load dropped at about 1.5% normalized deflection for the analysis results of CFST composite girder under positive bending moment (SC-P and FC-P specimen). This is because large cracks were developed between the steel tube and concrete slab during the analysis, and tensile stress decreased dramatically in this region during the analysis.

To investigate the effect of the degree of interaction between the CFST and concrete slab on the behavior of the CFST composite girder, additional finite element analyses were performed for FC-P specimen. Two different interface models were used to simulate the degree of the

Fig. 15. Crack pattern of the concrete infill of the FC-N specimen.

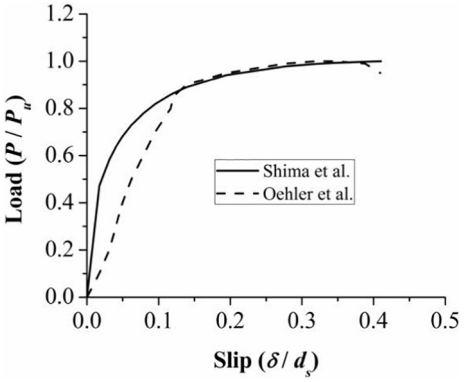

Fig. 17. Load-slip relationship curve proposed by previous researchers [25,26].

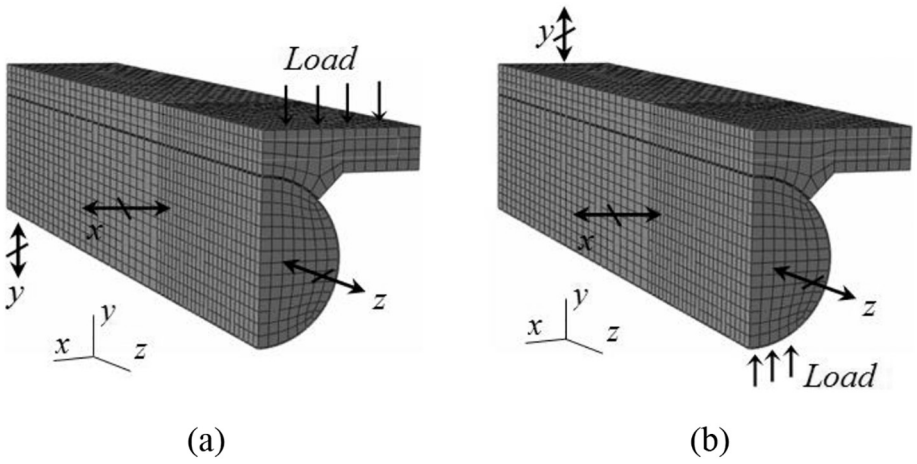

Fig. 18. Load and boundary conditions for the FE model: (a) Positive bending model; and (b) Negative bending model.

interaction. First interface model between the CFST and concrete slab was a 3 dimensional nonlinear spring model, where load-slip equation proposed by Shima & Watanabe [26] was applied (i.e. the first model is partial interaction model). The other one is a full interaction model so that all slip between the CFST and concrete slab is not permitted. The comparison results of analysis results with the test are shown in Fig. 18. From Fig. 20, it can be seen that the stiffness of the analysis model with the full interaction model is slightly higher than that of analysis model with the partial interaction model. However, the difference of the flexural strength between these two models is only 0.6%, and all analysis models agree well with the test results. As a result, the effect of the degree of interaction between the CFST and concrete slab was negligible for FC-P specimen, since the test specimen satisfies the condition of the full shear connection.

Figs. 21 (a) and (b) show the strain distributions in the mid-span along the height for the FC-P specimen (at 1.55% normalized deflection) and FC-N specimen (at 5.6% normalized deflection), respectively. The circles in Fig. 21 represent the test results, while the solid and dashed lines represent the strain in the steel tube and the concrete obtained from the analysis, respectively. The strain distributions obtained from the finite element analysis agrees well with those from the test, as shown in Fig. 21. Further, the location of NA obtained from the finite element analysis was also almost identical with that of the test results.

The crack patterns obtained from the finite element analyses were then compared with that from the test, as shown in Fig. 22. In the analysis, it is assumed that a crack is formed at the point that the maximum plastic principle strain is larger than zero [22]. From the results, the analysis results compared well with the test, as shown in Fig. 22. In

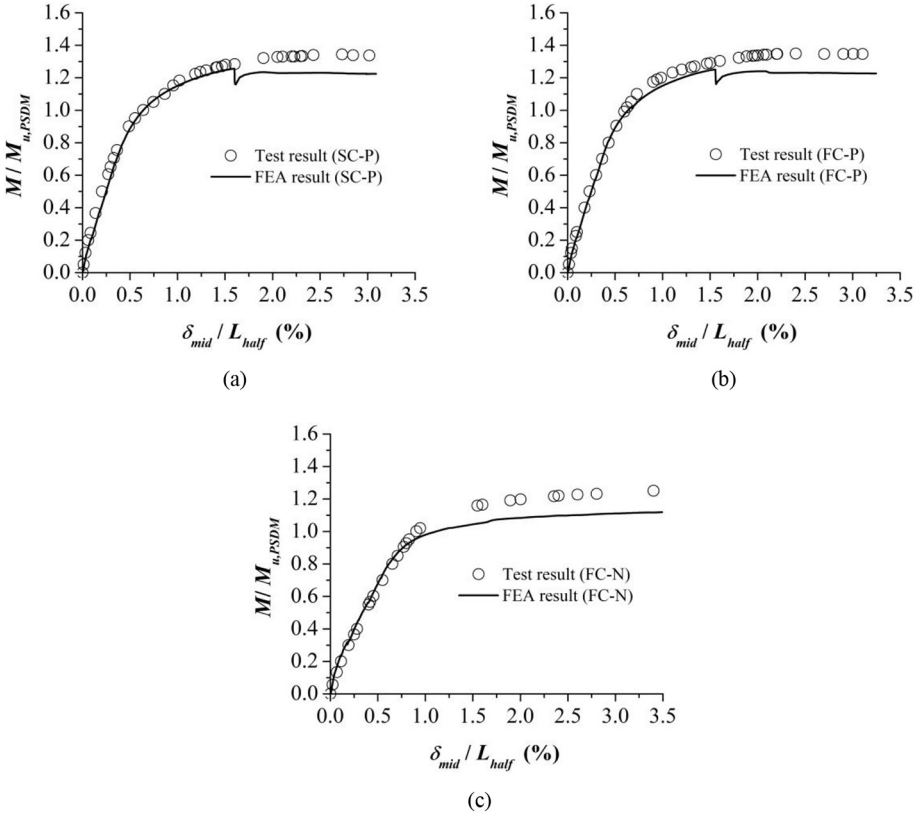

Fig. 19. Comparison of analysis results with test: (a) SC-P specimen; (b) FC-P specimen; and (c) FC-N specimen.

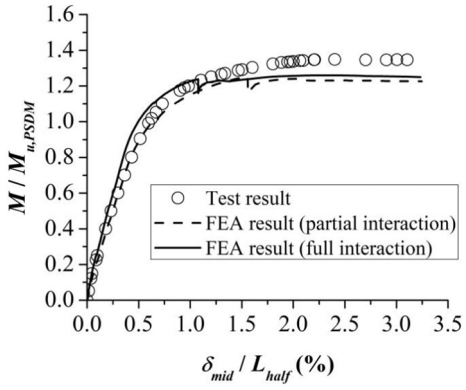

Fig. 20. Comparison of analysis results depending on the degree of interaction (FC-P).

summary, the developed finite element analysis model provided reasonable prediction of global (ex. moment-deflection relationship) and local (ex. strain distribution and crack pattern) responses of the CFST composite girder.

5. Parametric study and design consideration of the CFST composite girder

5.1. Description of models for parametric study

A series of parametric studies was conducted to investigate the effect of the D/t ratio, compressive strength of concrete infill, and local buckling of the tube (for negative bending moment) on the flexural strength of the CFST composite girder herein. These parameters were selected for the following reasons: (1) the steel tube in a CFST composite girder acts like a reinforcing bar in a reinforced concrete girder. The D/t ratio is

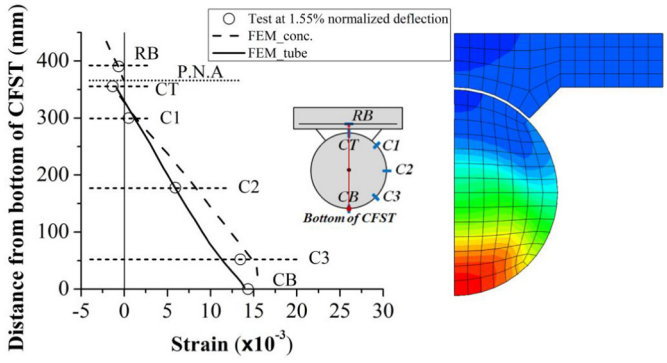

(a)

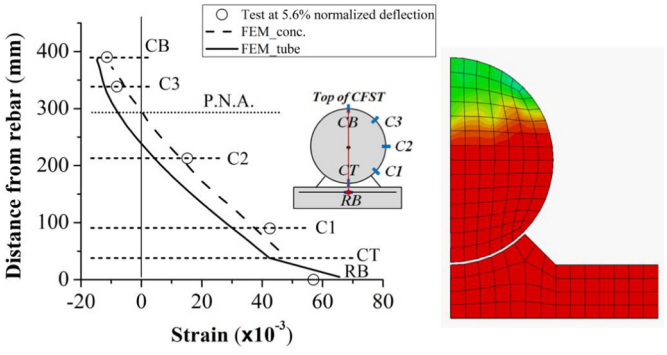

(b)

Fig. 21. Comparison of strain distribution with test: (a) the FC-P specimen; and (b) the FC-N specimen.

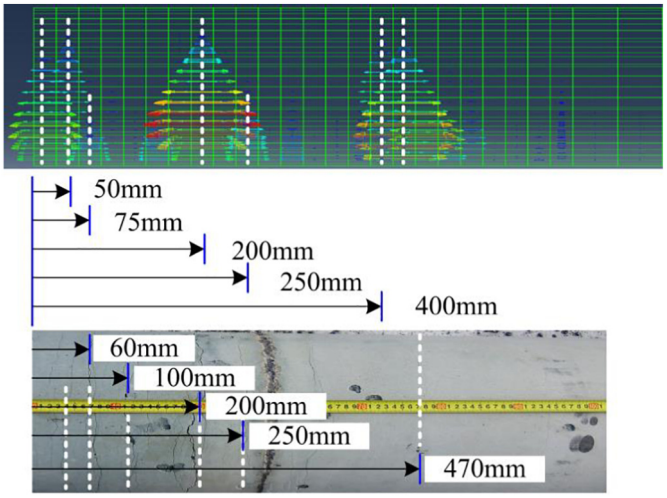

Fig. 22. Comparison of the crack pattern with test (FC-P specimen).

directly associated with the reinforcement ratio, and it affects the flexural behavior of the CFST composite girder. For example, a small D/t ratio may lead to brittle failure of the girder that is not desirable, since the concrete slab could be crushed before yielding of the steel tube due to an excessive amount of steel. (2) It is expected that the compressive strength of concrete infill may have an insignificant effect on the flexural strength of a CFST composite girder under positive bending, since the PNA may locate near the concrete slab due to the increased compression area that is added by the slab. Thus, it could be economical if the concrete infill could be replaced by low strength concrete, because the cost of the concrete is generally proportional to the strength. (3) For a CFST composite girder under negative bending, local buckling of the steel tube may occur, and it could affect the flexural strength of the CFST girder. Thus, it needs to be investigated.

The basic dimensions of the finite element models for parametric study were adopted to reflect the existing CFST composite girders. An outer diameter of 1000 mm and D/t ratio of 50–60 are commonly used in practice in South Korea. The effective width of the slab is usually designed as to be 1.5–2 times the external diameter of the CFST. AASHTO [19] recommends that the thickness of the slab should not be less than 175 mm, and the specified strength of the slab not be less than 28.0 MPa. These recommendations are adopted in this study. Based on these basic profiles of CFST composite girder, a total of 5 models were constructed (CFTG-R series in Table 2). In addition, 6 models (CFTG-L&S series in Table 2) having the same outer diameter with test specimens were also constructed to extend the test results for various D/t ratios and slab areas. The detail profiles of models used for the parametric study are shown in Table 2. Positive and negative bending moment

Table 2
Profiles of finite element models for the parametric studies.

Model	Slab (mm)		Steel tube (mm)		D/t	f_c' (MPa)		f_y (MPa)
	width	thick.	dia.	thick.		slab	infill	
CFTG-L40	700	90	355.6	9	40	24	24	320
CFTG-L79				4.5	79			
CFTG-L111				3.2	111			
CFTG-S40	550	60	355.6	9	40	24	24	320
CFTG-S79				4.5	79			
CFTG-S111				3.2	111			
CFTG-R40	1600	180	1000	25	40	28	28	320
CFTG-R59				17	59			
CFTG-R80				12.5	80			
CFTG-R100				10	100			
CFTG-R125				8	125			

were applied for the 11 models shown in Table 2. Further, additional 16 models were analyzed varying the compressive strength of the concrete infill ($f_{ci}'/f_{cc}' = 0, 0.25, 0.5$, and 1.25) for CFTG-S40, CFTG-S79, CFTG-R40, and CFTG-R80 models. Thus, a total of 38 models were analyzed. For the parametric study, four-point loading was applied to simulate pure bending. It is also noted that an elastic perfectly plastic material model was used for the steel tube, and the interface between the steel tube and concrete slab was perfectly bonded to each other.

5.2. Results of parametric study

From the analysis results, the PSDM underestimated the flexural strength of the CFST composite girder under both positive and negative bending moment by approximately 8–15% for the models shown in Table 3. Fig. 23 shows the relationship between the concrete compressive strain ε_{cc} in the extreme fiber of the concrete slab at the ultimate state and D/t ratio, where ε_{cc} was measured at the mid-span. It can be clearly seen that a smaller D/t ratio results in larger ε_{cc} at the ultimate state due to shifting of the PNA toward the center of the CFST (i.e. more compressive area is required with increasing the amount of steel). It is assumed that the concrete slab failed by compression when ε_{cc} is larger than 0.003, and could lead to brittle failure of the girder system. From the analysis results, ε_{cc} was larger than 0.003 when the D/t ratio less than 50 for the given models. Thus, care should be taken to determine the D/t ratio of the CFST composite girder to avoid brittle failure of the girder.

The effect of the compressive strength of the concrete infill on the flexural strength of the CFST composite girder is shown in Fig. 24. The x axis denotes the compressive strength ratio, f_{ci}'/f_{cc}', where f_{ci}' and f_{cc}' is the compressive strength of the infill and slab, respectively. The y axis in Fig. 24 represents the flexural strength of the CFST composite girder normalized by M_1, where M_1 denotes the flexural strength of the model with f_{ci}'/f_{cc}' equal to 1. From Fig. 24, it can be seen that the compressive strength of the infill has insignificant effect on the flexural strength of the CFST composite girder. However, the flexural strength of the girder without concrete infill (i.e. $f_{ci}'/f_{cc}' = 0$) was very low, since the steel tube at loading and boundary regions is severely distorted due to low bearing capacity. Thus, the steel tube must be filled to retain the cross section shape. However, the compressive strength of the concrete infill may not be important unless f_{ci}'/f_{cc}' is very low. For the given analysis models, the variation of flexural strength of the CFST composite girder was less than 5.5%, when f_{ci}'/f_{cc}' was larger than 0.25.

Local buckling of the CFST composite girder under negative bending moment could affect the flexural behavior, while the compression part of the steel tube doesn't buckle under positive bending moment, since the compression part of the steel tube is constrained on both sides by concrete infill and the slab. Thus, only the CFST composite girder under negative bending moment was considered to investigate the effect of local buckling on the flexural behavior. In AISC [12], filled composite sections are classified as compact, non-compact or slender depending on the D/t ratio, to take account of the effect of local bucking. The filled composite section is compact, when the D/t ratio is smaller than $\lambda_p = 0.09E_s/f_y$. If the D/t ratio is larger than λ_p, but does not exceed $\lambda_r = 0.31E_s/f_y$, the filled composite section is classified as non-compact. The section is slender, when the D/t ratio is larger than λ_r. In AISC [12], a slender section is not permitted as a flexural member. The CFST sections of the analyzed models were categorized (compact or non-compact) according to AISC D/t ratio limit [12] (Refer Table 3), and the validation of AISC provisions was examined for the CFST composite girder.

The analysis results for the CFST composite girder under negative bending moment are shown in Fig. 25, and Table 3. Comparative results show that the PSDM underestimated the flexural strength of the girder under negative bending moment by 6–12% for the given analysis

Table 3
Results of the parametric studies for the CFST composite girder under negative bending moment.

Model	λ_p	λ_r	D/t	Section,classification	$M_{u,FEM}/M_{u,PSDM}$
CFTG-L40	51	174	40	Compact	1.09
CFTG-L79			79	Noncompact	1.10
CFTG-L111			111	Noncompact	1.08
CFTG-S40	51	174	40	Compact	1.12
CFTG-S79			79	Noncompact	1.11
CFTG-S111			111	Noncompact	1.11
CFTG-R40	59	203	40	Compact	1.11
CFTG-R59			59	Compact	1.10
CFTG-R80			80	Noncompact	1.08
CFTG-R100			100	Noncompact	1.07
CFTG-R125			125	Noncompact	1.07

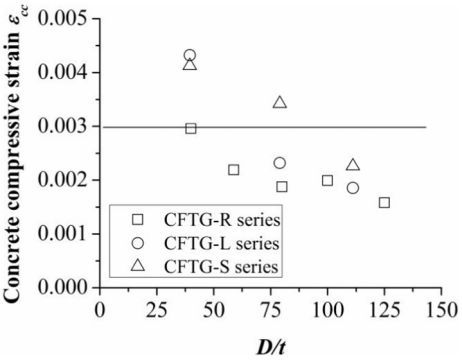

Fig. 23. Variation of ε_{cc} in the D/t ratio (for positive bending moment).

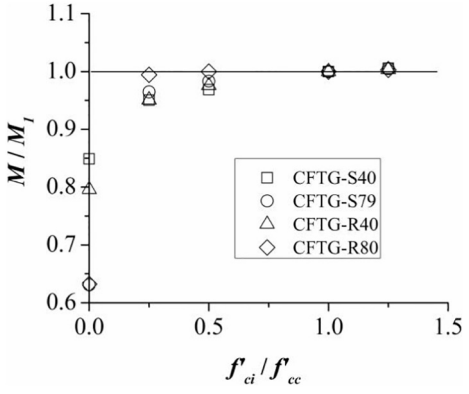

Fig. 24. Variation of $M_{u,FEM}/M_1$ in f_{ci}'/f_{cc}' (for positive bending moment).

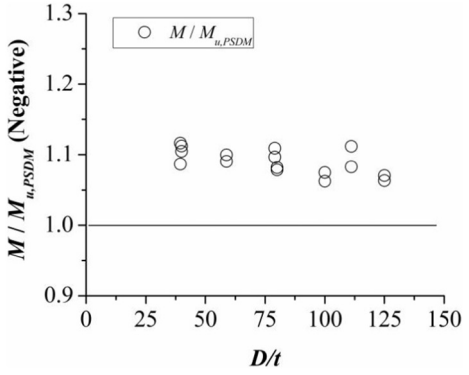

Fig. 25. Variation of the normalized flexural strength of the CFST composite girder under negative bending moment against the D/t ratio.

models, regardless of the classification of the section (compact or non-compact), even though the normalized flexural strength was slightly decreased with increasing D/t ratio (approximately 4% with increasing the D/t ratio up to 125). Unless the D/t ratio is extremely slender, the PSDM provides a reasonable estimation of the flexural strength of the CFST composite girder under negative bending moment.

6. Conclusion

The flexural strength of the CFST composite girder was investigated in this study. Based on the PSDM, simple equations to predict the flexural strength of the CFST composite girder were derived for both positive and negative bending moment. A series of experimental studies was then conducted. From the test results, the following observations were made:

(1) The proposed equations provided reasonable prediction of the flexural strength of the CFST composite girder, and the stress distribution obtained from the test is similar to that from the equation, even though partial interaction behavior was observed for the positive bending test.
(2) The effect of internal shear connectors between the steel tube and concrete infill on the flexural behavior of the CFST was negligible for the CFST composite girder under positive bending moment, since most of the concrete infill section experienced tension. However, the crack pattern of the concrete infill was affected by the existence of internal shear connectors.

A finite element analysis model was then developed, and a series of parametric studies was conducted. From the analysis results, the following conclusions were made:

(1) The proposed equations gave a reasonably conservative prediction (approximately 8% - 15%) of the flexural strength of the CFST composite girder under both positive and negative bending moment.
(2) With decreasing the D/t ratio, the compressive strain at the extreme fiber of the concrete slab, ε_{cc}, increased, and this is not desirable, since brittle compression failure could occur. For the analysis models with a D/t ratio less than 50, ε_{cc} exceeded 0.003.
(3) The concrete infill is necessary to retain the original shape of the steel tube at the support and loading region. However, the compressive strength of infill has insignificant effect on the flexural strength of the CFST composite girder when f_{ci}'/f_{cc}' was larger than 0.25 for the given analysis models.
(4) Unless the D/t ratio is extremely slender, the PSDM provides a reasonable estimation of the flexural strength of the CFST composite girder under negative bending moment.

Acknowledgements

This research was supported by research grant from National Research Foundation of Korea (NRF) (2018R1D1A3B07047459) and Kangwon National University.

Appendix A. Appendix I

The flexural strength of CFST composite girder is as follows:
(1) Case 1

$$M_u = 0.85 f_{cc}{}' b_e a \ (R + y_c - 0.5a)$$

The equilibrium equation to obtain a is given by

$$0.85 f_{cc}{}' b_e a = 2\pi \ t \ r_m f_y$$

(2) Case 2

$$M_u = 0.85 f_{cc}{}' b_e t_c (y_2 + R - G_s) + 2\pi \ t \ r_m f_y G_s + A_b f_{yr} (G_d - G_s).$$

in which

$$G_s = \frac{2R}{3}\left(\frac{\sin^3\theta}{\theta - \sin\theta \ \cos\theta}\right)$$

The equilibrium equation to obtain θ is given by

$$0.85 f_{cc}{}' b_e t_c + A_b f_{yr} + 2R^2(\theta - \sin\theta \ \cos\theta) f_y = 2\pi t r_m f_y$$

where, A_b is the area of reinforcing bar, and f_{yr} is the yield stress of the reinforcing bar.
(3) Case 3 and Negative moment region

$$M_u = 0.85 f_{cc}{}' b_e t_c (y_2 + R) + 4 t r_m \theta f_y G_s + 0.95 r_i^2 (\theta - \sin\theta \ \cos\theta) f_{ci}{}' G_i + A_b f_{yr} G_d$$

in which,

$$G_s = \frac{r_m \ \sin\theta}{\theta}$$

$$G_i = \frac{2r_i}{3}\left(\frac{\sin^3\theta}{\theta - \sin\theta \ \cos\theta}\right)$$

For the negative moment region, f_{cc}' should be zero. The equilibrium equation to obtain θ is given by.

$$0.85 f_{cc}{}' b_e t_c + A_b f_{yr} + 4 t r_m \theta f_y + 0.95 r_i^2 (\theta - \sin\theta \ \cos\theta) f_{ci}{}' = 2\pi t r_m f_y$$

References

[1] H.T. Hu, C.S. Huang, M.H. Wu, Nonlinear analysis of axially loaded concrete-filled tube columns with confinement effect, J. Struct. Eng. 129 (10) (2003) 1322–1329.
[2] H. Lu, L.H. Han, X.L. Zhao, Analytical behavior of circular concrete-filled thin-walled steel tubes subjected to bending, Thin-Walled Struct. 47 (2009) 346–358.
[3] Z.Y. Shen, M. Lei, Y.Q. Li, Z.Y. Lin, J.G. Luo, Experimental study on seismic behavior of concrete-filled L-shaped steel tube columns, Adv. Struct. Eng. 16 (2013) 1235–1247.
[4] Bishop ES. Evaluation of the flexural resistance and stiffness models for circular concrete-filled steel tube members subjected to combined axial-flexural loading. A Thesis Submitted in Partial Fulfillment of Master of Science in Civil Engineering, University of Washington Seattle, WA
[5] J. Moon, C.W. Roeder, D.E. Lehman, H.E. Lee, Analytical modeling of bending of circular concrete-filled steel tubes, Eng. Struct. 42 (2012) 349–361.
[6] B.C. Chen, T.L. Wang, Overview of concrete filled steel tube arch bridges in China, Pract. Period. Struct. Des. Constr. 14 (2) (2009) 70–80.
[7] S. Nakamura, Y. Momiyama, T. Hosaka, K. Homma, New technologies of steel/concrete composite bridges, J. Constr. Steel Res. 58 (2002) 99–130.
[8] J.Y. Kang, E.S. Choi, W.J. Chin, J.W. Lee, Flexural behavior of concrete-filled steel tube members and its application, Int. J. Steel Struct. 7 (2007) 319–324.
[9] T. Hosaka, S. Nakamura, T. Umehara, K. Nishiumi, Design and experiments on a new railway bridge system using concrete filled steel pipes, Composite Construction, Conventional and Innovative: Conference Report 1997, pp. 367–372.
[10] S. Nakamura, H. Tanakab, K. Kato, Static analysis of cable-stayed bridge with CFT arch ribs, J. Constr. Steel Res. 65 (2009) 776–783.
[11] K. Yoshida, Y. Taira, Y. Niihara, Y. Hishiki, T. Tominaga, Strength of composite girder for new type cable-stayed bridge, IABSE Symposium Report, IABASE Conference : Cable-Supported Bridges - Challenging Technical Limits. Seoul June, 2001, pp. 25–32.
[12] American Institute of Steel Construction (AISC), Specification for Structural Steel Buildings, AISC, Chicago, 2010.
[13] C.W. Roeder, D.E. Lehman, E. Bishop, Strength and stiffness of circular concrete-filled tubes, J. Struct. Eng. 136 (12) (2010) 1545–1553.
[14] A.D. Probst, T.H.K. Kang, C. Ramseyer, U. Kim, Composite flexural behavior of full-scale concrete-filled tubes without axial loads, J. Struct. Eng. 136 (11) (2010) 1401–1412.
[15] H.G.L. Prion, J. Boehme, Beam-column behaviour of steel tubes filled with high strength concrete, Can. J. Civ. Eng. 21 (1994) 207–218.
[16] M. Elchalakani, X.L. Zhao, R.H. Grzebieta, Concrete-filled circular steel tubes subjected to pure bending, J. Constr. Steel Res. 57 (11) (2001) 1141–1168.

[17] L.H. Han, H. Lu, G.H. Yao, F.Y. Liao, Futher study on the flexural behaviour of concrete-filled steel tubes, J. Constr. Steel Res. 62 (6) (2006) 554–565.
[18] M. Elchalakani, X.L. Zhao, R.H. Grzebieta, Concrete-filled steel circular tubes subjected to constant amplitude cyclic pure bending, Eng. Struct. 26 (14) (2004) 2125–2135.
[19] American Association of State Highway and Transportation Officials (AASHTO), AASHTO LRFD Bridge Design Specifications, 4th edition AASHTO, Washington, DC, 2007.
[20] D.J. Oehlers, M.A. Bradford, Composite Steel and Concrete Structural Members: Fundamental Behaviour, Pergamon Press, Oxford, 1995.
[21] L.H. Han, G.H. Yao, Z. Tao, Performance of concrete-filled thin-walled steel tubes under pure torsion, Thin-Walled Struct. 45 (2007) 24–36.
[22] ABAQUS, Abaqus Analysis user's Manual Version 6.10. Dassault Systèmes Simulia Corporation, Providence, 2010.
[23] P. Baltay, A. Gjelsvik, Coefficient of friction for steel on concrete at high normal stress, J. Mater. Civ. Eng. 2 (1) (1990) 46–49.
[24] T.T.C. Hsu, Y.L. Mo, Unified Theory of Concrete Structures, John Wiley & Sons Ltd, Chichester, 2010.
[25] D.J. Oehler, C.G. Coughlan, The shear stiffness of stud shear connections in composite beams, J. Constr. Steel Res. 6 (1986) 273–284.
[26] H. Shima, S. Watanabe, Formulation for load-slip relationships of headed stud connector, Proceedings of 34th International Symposium on Bridge and Structural Engineering. Venice Sept, 2010, pp. 69–76.